Christopher L. Holloway, Matthew T. Simons, Abdulaziz H. Haddab, Joshua A. Gordon, David A. Anderson, Georg Raithel, and Stephen D. Voran

A Multiple-Band Rydberg Atom-Based Receiver

AM/FM stereo reception.

xxxxx

With the redefinition of the International System of Units (SI) that occurred in November 2018, there has been much attention on the development of atom-based sensors for metrology applications that are directly linked to the SI. In particular, great progress has been made in using Rydberg atom-based techniques for electric field (E-field) metrology. These Rydberg atom-based E-field sensors have made it possible to develop atom-based receivers, which potentially have many benefits over conventional technologies in detecting and receiving modulated signals.

In this article, we describe the multichannel atom-based reception of both amplitude modulation (AM) and frequency modulation (FM) signals. We demonstrate this using two different atomic species to detect and receive AM and FM signals in stereo. We also investigate the effect of Gaussian noise on the ability to receive AM and FM signals. These results illustrate the simultaneous multichannel receiving capability of an atom-based receiver to produce high-fidelity stereo reception from both AM and FM signals. This article shows an interesting way of applying the relatively newer (and sometimes esoteric) fields of quantum optics and atomic physics to the century-old topic of radio reception.

Digital Object Identifier 10.1109/MAP.2020.2976914
Date of current version: 2 April 2020

INTRODUCTION

Rydberg atoms are atoms with one or more electrons excited to a very high principal quantum number n [1]; these atoms have several useful properties that scale as n. In particular, from an electric E-field viewpoint, they have very large dipole moments, which scale as n^2. These large dipole moments render them highly sensitive to E-fields, making for good field sensors and detectors.

We and others have made great strides in the development of new radio-frequency (RF) E-field strength and power metrology techniques based on the large dipole moments associated with the Rydberg states of alkali atomic vapor [either cesium-133 (^{133}Cs) or rubidium-85 (^{85}Rb)] placed in glass cells [2]–[20]. In this approach, the phenomenon of electromagnetically induced transparency (EIT) is used for the E-field sensing. These measurements can be performed either when the RF field is on-resonance with a Rydberg transition [using Autler–Townes (AT) splitting] [2]–[7] or off-resonance (using ac Stark shifts) [12] or, more generally, by using a Floquet method [11].

The on-resonance EIT/AT method allows for the detection of fields from tens of megahertz to 1 THz. The Stark shift approach allows for the detection of fields down to dc. However, this latter approach requires relatively high field strengths compared to the EIT/AT approach. The article concentrates on the EIT/AT approach. These Rydberg atom techniques allow for the development of an E-field probe that does not require a calibration (since an absolute value of the field is determined by the atomic properties of the Rydberg atom itself) and provide a self-calibrating, direct SI-traceable method for RF E-field metrology.

This Rydberg atom-based sensor can also act as a compact receiver. Specifically, Rydberg atoms can lead to the development of a quantum-based receiver that measures the amplitude, phase, and polarization of modulated E-fields over a frequency range of hundreds of megahertz to 1 THz. Research into using Rydberg atoms to receive AM and FM signals is new, with demonstrations given in [21]–[26]. This has led to the new term *atom radio*, coined in [23] and [27]. Recently, we extended the atom receiver to develop a Rydberg atom-based mixer that allows for the measurement of the phase of an RF wave [28], which was the needed missing link for Rydberg atom-based quantum sensors to be able to fully characterize the RF E-field in one compact vapor cell. These phase measurements allow for detecting and receiving digitally modulated communication-type signals [29].

Along with others (as discussed in the following paragraphs in this section), one of the interesting possibilities for this new technique is the ability to have a multiple-band (or multiple-channel) receiver in a single atomic vapor cell. In this article, we demonstrate a multichannel Rydberg atom-based receiver by realizing AM/FM stereo reception with atomic vapor. To clarify, in its strictest sense, *multiband* implies using frequencies in different frequency bands, and *multichannel* implies different frequencies in the same frequency band. (Here, we use two frequencies in the K band). The Rydberg atom approach has enough bandwidth that either approach could be used; thus, we use the two terms (*band* and *channel*) interchangeably here.

Current RF systems use complex integrated circuits and metallic structures to couple, capture, demodulate, and convert signals transmitted on RF E-fields to currents and voltages. The state-of-the-art receiver technology relies on complex circuits, mixers, amplifiers, and digitizers to receive, demodulate, and decode signals. The systems are also heavily band limited and size limited in comparison to what a Rydberg atom receiver could accomplish. In addition, RF systems are limited to frequency bands defined by the waveguide structures within them. For example, the best metrology-grade vector network analyzers operate up to approximately 50 GHz, after which external frequency extenders are required. These operate only at discrete frequency bands, such as WR-08 (90–140 GHz) and WR-05 (140–220 GHz), requiring a large amount of equipment to operate at frequencies between 1 GHz and 1 THz. Current systems also require frequent calibration.

In contrast, Rydberg atoms could be used to realize a single receiver that can span the range from hundreds of megahertz to 1 THz, is very compact (much smaller than the RF operating wavelength), is more sensitive than current receivers, can be self-calibrated, and can be readily included in a grander quantum communications and information architecture. Over the range of hundreds of megahertz to 1 THz, the large dipole moments of Rydberg atoms make possible atomic sensors that can be orders of magnitude smaller than the RF wavelength. At 1 GHz, classical antennas are on the order of 300 mm in size, whereas the active region of a Rydberg atom sensor typically ranges between 0.1 mm and 10 mm in size. Furthermore, using the EIT/AT technique in preliminary tests has shown that Rydberg atoms not only respond strongly to E-fields over the 1-THz range but also inherently demodulate time-varying signals without the need for external mixers, thereby simplifying the receiver architecture. All of these attributes suggest that it is possible to make a Rydberg atom receiver that is subwavelength, compact, very broadband, and sensitive and that can by itself achieve what currently requires many pieces of electronic equipment.

These atom-based receivers can offer the following advantages over current technologies:

- nanosized sensor and receivers
- the fact that atom-based sensors have the same bandwidth response over the entire frequency range of 100 MHz–1 THz
- direct real-time readout
- no need for traditional demodulation electronics because the atoms automatically perform the demodulation
- multiband (or multichannel) operation in one compact vapor cell
- the possibility of electromagnetic interference-free receiving
- ultrahigh sensitivity reception from 100 MHz to 1 THz.

When all is said and done, the possibility of a chip-scale multiband atom receiver is not that far off in the future. Other chip-scale atomic devices (including clocks) have already been realized [30], [31].

One benefit of the Rydberg atom-based E-field measurement technique is that it is a broadband sensor: with one sensor, it is possible to detect RF E-fields from a few hundred megahertz to 1 THz. There are various ways to take advantage of this to achieve a multichannel receiver with Rydberg atoms, in effect, receiving multiple communication channels simultaneously. One can use one atomic species (say, ^{133}Cs or ^{85}Rb) and different laser wavelengths (explained in the next section) to receive different signals (or different communication channels) simultaneously, where each channel corresponds to a different laser wavelength. This approach will be the topic of a future publication.

The approach we discuss here is based on using two atomic species (^{133}Cs and ^{85}Rb) simultaneously, where each atomic species detects and receives a separate communication channel. This allows for two independent sets of data to be received at the same time. We demonstrate this by transmitting, detecting, receiving, and playing (recording) a musical composition in stereo. We also investigate the effect of background noise on the ability to receive the audio signal.

DESCRIPTION OF THE RYDBERG ATOM-DETECTION TECHNIQUE

To use Rydberg atoms as an AM/FM receiver, we leverage recent work in the development of a new atom-based,

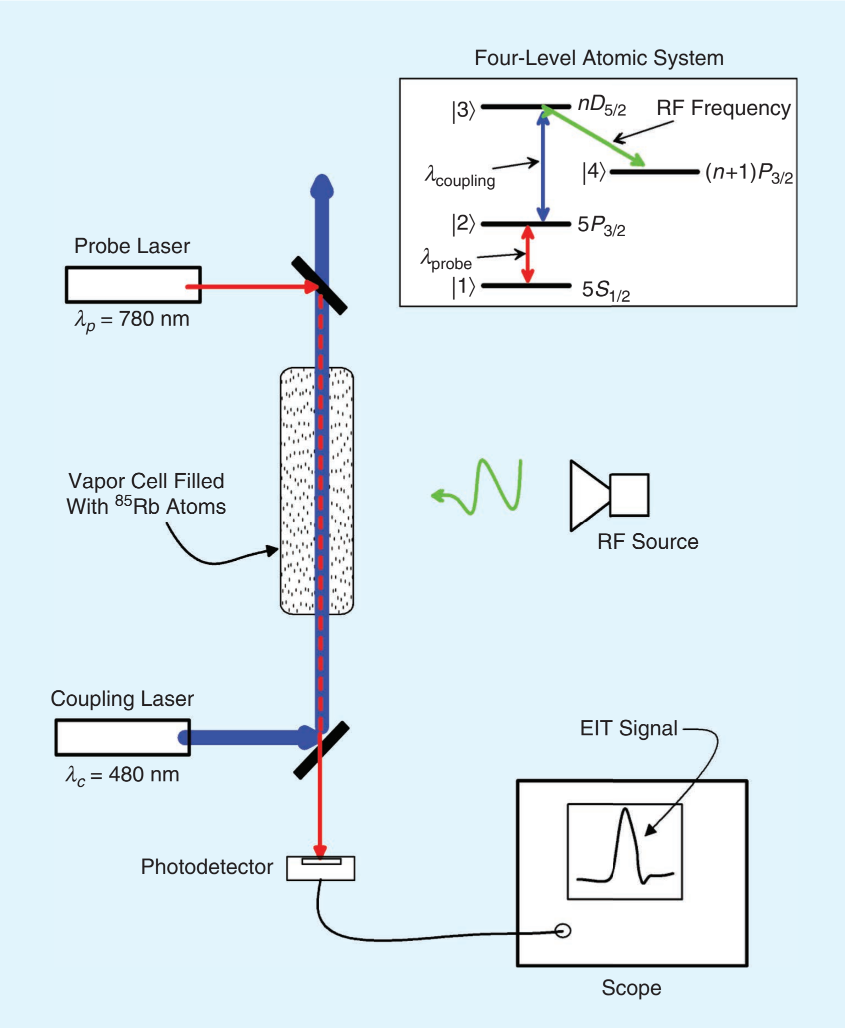

FIGURE 1. A four-level system and the vapor cell setup for measuring EIT, with a counterpropagating probe and coupling beams. This figure shows only ^{85}Rb, but ^{133}Cs is explained in the same way.

SI-traceable approach for determining RF E-field strength [2]–[20]. In this approach, the response of a vapor of alkali atoms (excited to a high-energy, or "Rydberg," state) to an external RF field is detected with a probe laser. The atoms are excited through a two-step process, where the probe laser also serves to couple the ground state of the atoms to an intermediate state (see the inset in Figure 1). A second coupling laser is used to couple the intermediate state to the Rydberg state. The presence of this coupling laser results in a coherence that causes a decrease in the absorption of the probe laser when both lasers are on resonance.

This effect is known as *EIT*. To establish EIT, both lasers must overlap through a vapor cell containing the alkali atoms, as shown in Figure 1. When the atoms are excited to a high-energy Rydberg state, they are very sensitive to RF fields, and this effect is enhanced if the RF field is resonant with an atomic transition (Figure 1 inset). The presence of an external RF field, then, alters the transmission spectrum of the probe laser, which can be used to either measure the strength or detect a modulation of the RF E-field.

In effect, the detection scheme is basically an atomic spectroscopy measurement. To obtain the probe-laser transmission spectrum, either the wavelength of the probe laser or the coupling laser can be scanned. Figure 2 shows an example of an EIT signal (the curve with one peak centered at $\Delta_p = 0$ and labeled as "RF Off") for the case of scanning the probe laser (where $\Delta_p = \omega_p - \omega_o$; ω_p is the angular frequency of the probe laser, and ω_o is the on-resonance angular frequency of the Rydberg state transition). To obtain these results, we used ^{85}Rb atoms and scanned the probe laser across the D_2 transition ($5S_{1/2} - 5P_{3/2}$ or wavelength of $\lambda_p = 780.24$ nm [36]).

The four levels of the atomic system $|1\rangle, |2\rangle, |3\rangle$, and $|4\rangle$ correspond, respectively, to the ^{85}Rb $5S_{1/2}$ ground state, $5P_{3/2}$ excited state, and two Rydberg states (levels 3 and 4). The coupling laser is locked to the $5P_{3/2} - 47D_{5/2}$ ^{85}Rb Rydberg transition ($\lambda_c = 480.271$ nm). We used a lock-in amplifier to enhance the EIT signal-to-noise ratio by modulating the coupling-laser amplitude with a 30-kHz square wave. This removes the background and isolates the EIT signal.

When a third electromagnetic field (the RF field), tuned to another Rydberg atomic transition (levels 3 and 4), is present, the original transparency region (the center EIT signal in Figure 2) is split into two regions separated in frequency (AT-splitting); this is illustrated by the two other curves in Figure 2. These two results are for two different RF-field strengths at 20.64 GHz (corresponding to the transition between Rydberg states $47D_{5/2}$ and $48P_{3/2}$). The AT splitting increases with increasing applied E-field strength. The frequency separation is directly related to the strength of the RF E-field by the following [3], [4], [14], [15]:

$$|E| = 2\pi \frac{\hbar}{\wp} \frac{\lambda_p}{\lambda_c} \Delta f_m \quad \text{scanning probe laser}$$
$$|E| = 2\pi \frac{\hbar}{\wp} \Delta f_m \quad \text{scanning coupling laser,} \qquad (1)$$

where Δf_m in the measured frequency separation between the two peaks, $\hbar$ is Planck's constant, and $\wp$ is the atomic dipole moment of the RF transition. A ratio of wavelengths is needed when the probe laser is scanned [14], [15].

In determining the operational carrier frequency of the Rydberg atom-based sensor, it is important to note that Rydberg atom behavior is fundamentally different from that of a conventional antenna. A conventional antenna uses geometry to tune (and/or impedance-match) to determine the carrier frequency range, and a tuner selects a carrier frequency value. That is, a conventional antenna/radio unit is typically designed for one particular operational frequency.

The Rydberg sensor, however, uses different atomic states to detect the E-field and, in turn, the wavelength of the coupling laser determines the operational carrier frequency. That is, the wavelength of the coupling laser determines the atomic state and defines the frequency that will be measured. (See [3] for more details.) This allows for a large selection of discrete carrier frequencies spread out over a wide range. Different carriers are accessed by changing the wavelength of the coupling laser.

Since the E-field strength is directly related to Planck's constant, it is a direct SI-traceable, self-calibrated measurement. This feature of SI traceability is the result of Planck's constant becoming an SI-defined quantity in November 2018 through the redefinition of the SI [32], [33]. The measurement of the E-field strength requires only the atomic dipole moment $\wp$ (a parameter that can be calculated very accurately [3], [17]) and a relative optical frequency measurement (Δf_m, which can be measured very accurately and is calibrated to the hyperfine atomic structure [5]).

Using (1) and the measured frequency separation Δf_m, the E-field can be determined. These calculated E-field values are also shown in Figure 2, which requires a calculation for $\wp$. The dipole moment for this RF transition is calculated to be $\wp = 1386.7\, ea_0$ (where e is the elementary charge, and a_0 is the Bohr radius, or $a_0 = 0.529177 \times 10^{-10}$ m), which includes a radial part of $2830.6\, ea_0$ and an angular part of 0.48989 (corresponding to collinear polarized RF and optical fields). For discussion on determining $\wp$ for various atomic states, see [3] and [17]. The atomic dipole moment can be determined to less than 0.1%, which has been verified experimentally [17].

The EIT/AT signal can also be monitored for changes in the RF field strength. In the following sections, we describe how this can be used to receive modulated RF signals through changes in the probe-laser transmission.

DETECTING AN AM/FM SIGNAL

Before we discuss the detection scheme for AM/FM-modulated signals, we first must consider the behavior of the EIT signal just before it splits. A minimum RF field level is required before the splitting shown in Figure 2 occurs. When an RF field is incident onto the vapor cell and its field strength is increased from zero, the amplitude of the EIT signal decreases, and its linewidth broadens before the EIT signal starts to split [4]. This is illustrated in Figure 3(a), which shows the EIT signal with no RF field and three cases for different RF field strengths. The curve labeled "Field Level 3" corresponds to a field strength high enough to cause splitting.

We discuss two possibilities for the detection of both AM and FM signals. One is based on detection of the EIT signal at $\Delta_p = 0$, and one on detection at $\Delta_p \neq 0$. They both work basically the same way, and choosing one versus the other depends on the power in the RF carriers and the modulation depth used. Recall that an AM signal is basically a carrier for which the amplitude of the carrier changes. Let us start by discussing the situation where the amplitude of the carrier (and the modulation depth) is such that no splitting in the EIT signal will occur.

The AM carrier will cause the peak of the EIT line to move only up and down the dashed line shown in Figure 3(a). Therefore, if the probe laser is locked to $\Delta_p = 0$ (while the coupling laser is also locked to the $5P_{3/2} - 47D_{5/2}$ Rydberg transition), the voltage output of the photodetector (used to measure the probe-laser transmission) would be directly correlated to the modulating signal. That is, no demodulation circuity is needed, the Rydberg atoms (via the probe transition through the cell) automatically demodulate the signal, and we get a direct readout of the baseband signal. How the atoms actually perform the demodulation is discussed at the end of the "Experimental Setup for AM/FM Stereo Receiver" section.

When the carrier frequency signal strength is large enough to split the EIT line into two peaks, AM causes the EIT peaks to move left to right (or right to left). This in illustrated in Figure 3(b), which shows (on a zoomed-in x-axis) the peak of one of the EIT lines (the one to the left) for different values of the carrier-signal amplitude. Here, again, if the probe laser is locked to $\Delta_p = -2\pi{\cdot}8$ MHz (while the coupling laser is locked to the $5P_{3/2} - 47D_{5/2}$ Rydberg transition), the voltage output of the photodetector [following the dashed line in Figure 3(b), which corresponds to the EIT signal strength] will be directly correlated to the modulating signal (i.e., the atom's response basically modulates the photodetector signals). We could just as well lock the probe laser to a wavelength just off the peak when determining the modulated signal.

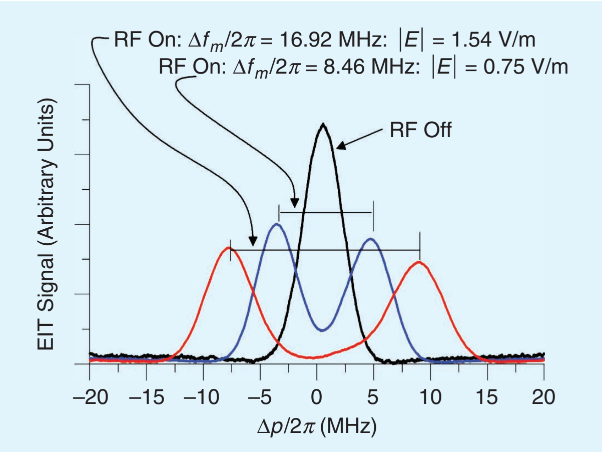

FIGURE 2. The EIT signal (i.e., probe-laser transmission through the cell) as a function of probe-laser detuning Δ_p. This data set is for 20.64 GHz and corresponds to the following four-level ^{85}Rb atomic system: $5S_{1/2} - 5P_{3/2} - 47D_{5/2} - 48P_{3/2}$. A similar curve appears in [35].

The detection of an FM signal works in a similar manner. When an RF field is detuned (i.e., the RF frequency is changed) from its resonant RF transition frequency, it has two main effects on the observed splitting of the EIT signal, discussed in detail in [16] [see Figure 3(c) and (d)]. First, the two peaks of the EIT signal are nonsymmetric (i.e., the heights of the two peaks are not the same). The second effect of RF detuning is that the separation between the two peaks increases with RF detuning. If the probe laser is locked to some Δ_p (while the coupling laser is locked to the $5P_{3/2} - 47D_{5/2}$ Rydberg transition), the voltage output of the photodetector (see the EIT signal strength along the dashed line) will be directly correlated to the modulating signal (i.e., the atom's response basically modulates the photodetector signals).

EXPERIMENTAL SETUP FOR AN AM/FM STEREO RECEIVER

The experimental setup for transmitting, detecting, receiving, playing (through a set of speakers), and recording a musical composition in stereo is shown in Figure 4. We first discuss the AM scheme. We chose a musical composition with both instrumental and vocal parts as the data to transmit and receive via the multichannel Rydberg atom receiver [Figure 5(a)] [34]. We separated these two parts into two different audio data files and saved them in the .wav format; we used the open source

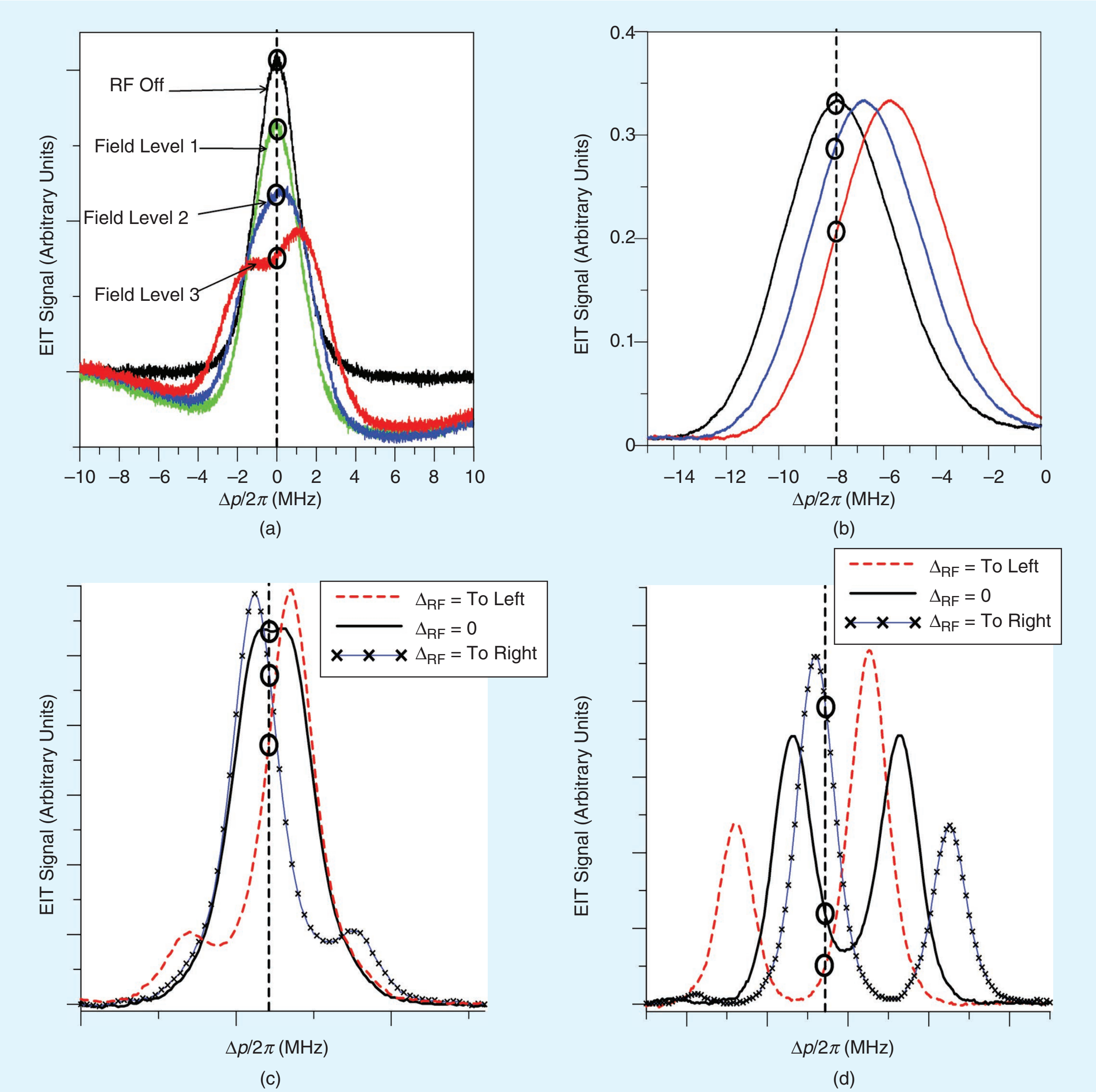

FIGURE 3. The detection scheme for an AM/FM signal: (a) the AM monitoring at the center of the EIT signal, (b) the AM monitoring on one of the side peaks of the split EIT line, (c) an FM monitoring scheme when little splitting is present, and (d) an FM monitoring scheme with well-defined splitting.

program Audacity (mentioning this product does not imply an endorsement by the National Institute of Standards and Technology [NIST] but serves to clarify the software used) to play these two audio files.

The instrumental part was put on the left channel, and the vocal part was put on the right channel of the headphone jack of the computer. The output of the headphone jack is a voltage waveform with a range of ±1 V. These two voltage waveforms were used to modulate two different carrier frequencies. The left channel modulated a 19.626-GHz carrier, and the right channel modulated a 20.644-GHz carrier. We used two different signal generators (SGs) to generate these two different continuous-wave (CW) signals. The modulation was performed using the internal AM/FM feature in the SG, which is limited to 100 kHz. However, since the waveform for an audio file is limited to approximately 20 kHz, this limit is not an issue in the data presented here.

The output from each SG was connected to two Narda 638 standard-gain horn antennas (mentioning this product does not imply an endorsement by NIST but serves to clarify the antennas used). Each antenna was placed 30 cm from a cylindrical glass vapor cell of 75-mm length and 25-mm diameter containing both ^{85}Rb and ^{133}Cs atomic vapor [Figure 4(a) and (b)]. The input power levels to the horn antennas were –14.2 dBm for the 19.626-GHz carrier and –22.0 dBm for the 20.644-GHz carrier.

The two atom species require the use of four lasers; the setup shown in Figure 4(b) was used to detect and receive the modulated signals. The ^{85}Rb atoms are used to receive the 20.644-GHz modulated carrier, and the ^{133}Cs atoms are used to receive the 19.626-GHz modulated carrier. The probe laser for ^{85}Rb is a 780.24-nm laser focused to a full width at half maximum (FWHM) of 750 μm, with a power of 22.3 μW. To produce an EIT signal in ^{85}Rb (using the atomic states given in Figure 1), we apply a counterpropagating coupling laser

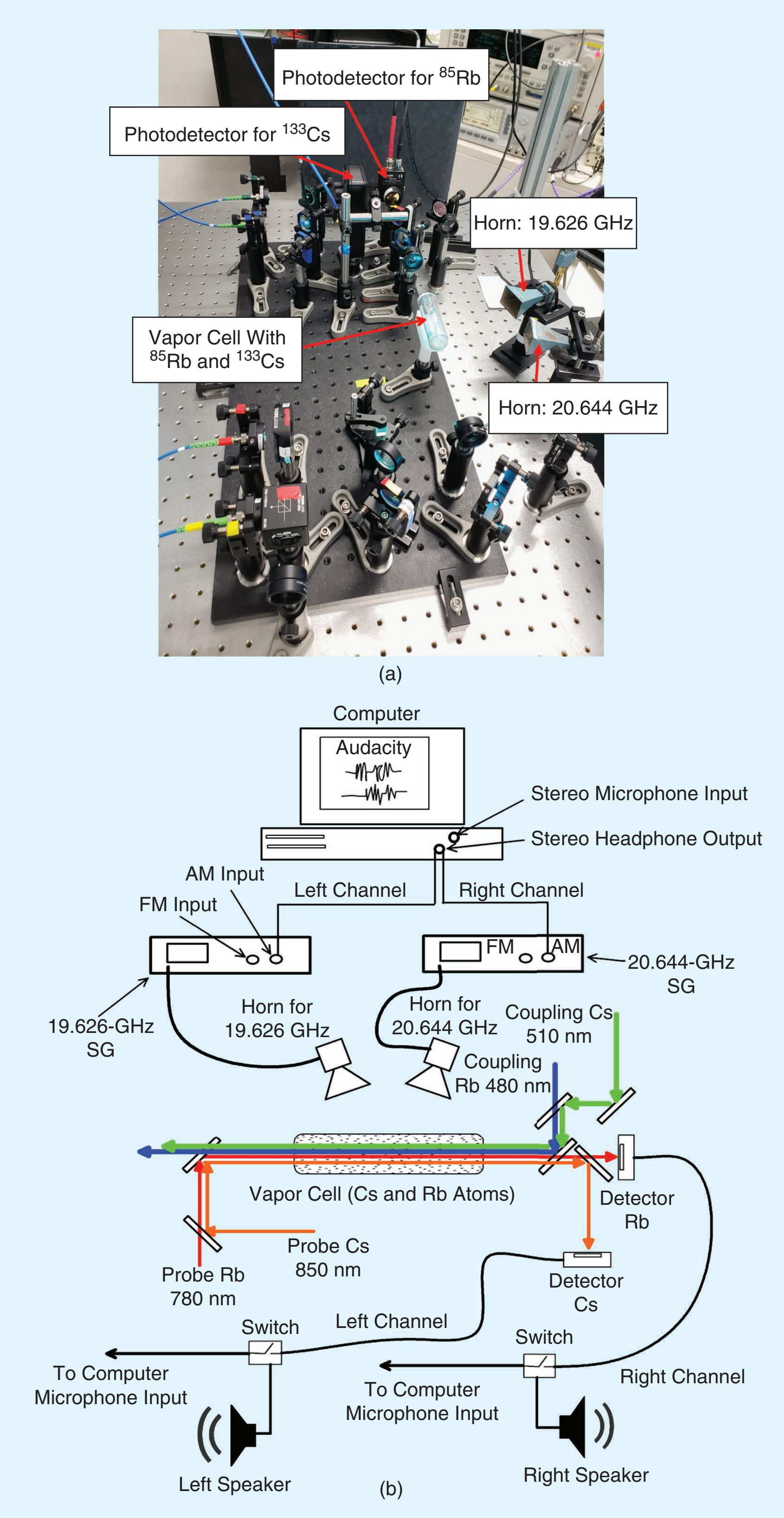

FIGURE 4. An experimental setup for AM/FM receiver measurements using EIT: a) a photo and (b) a block diagram of the setup, including the vapor-cell setup for two atomic species and four lasers (two counterpropagating probe beams and two coupling beams). (Source: NIST; used with permission.)

(wavelength $\lambda_c = 480.271$ nm) with a power of 43.8 mW, focused to a FWHM of 250 μm. The probe for ^{133}Cs is a 850.53-nm laser ($6S_{1/2} - 6P_{3/2}$) focused to an FWHM of 750 μm, with a power of 41.2 μW. To produce an EIT signal, we couple to the ^{133}Cs $6P_{3/2} - 34D_{5/2}$ states by applying a counterpropagating coupling laser at $\lambda_c = 511.1480$ nm with a power of 48.7 mW, focused to an FWHM of 620 μm. We apply an RF field at 19.626 GHz to couple states $34D_{5/2}$ and $35P_{3/2}$.

Two different photodetectors were used to detect the transmission for each probe laser through the vapor cell (one for ^{85}Rb and one for ^{133}Cs). The output of the photodetectors is a voltage

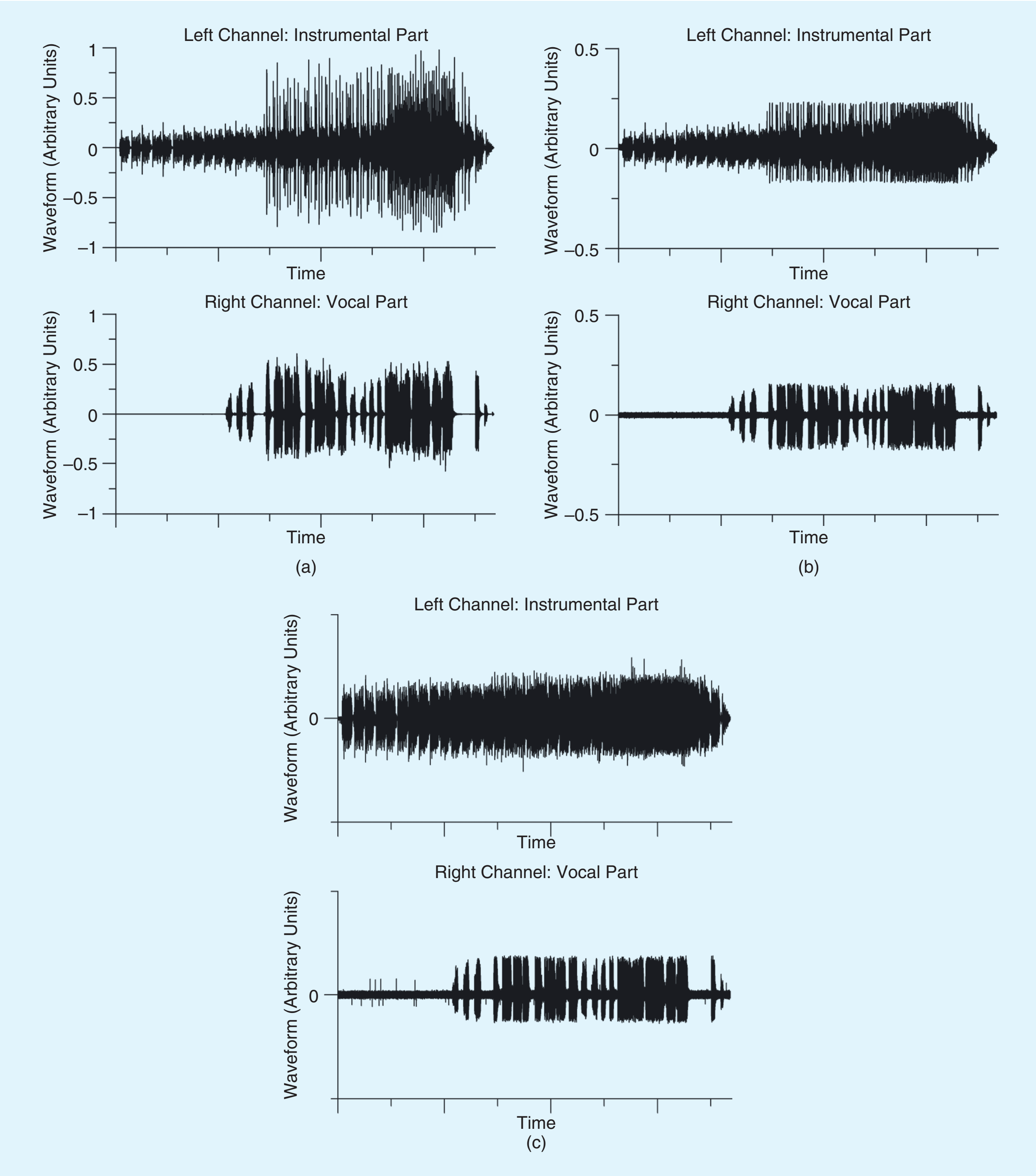

FIGURE 5. (a) The waveform of the musical composition used for the stereo AM/FM receiving experiments, (b) the received waveform of the musical composition from the AM scheme for the atom-based stereo receiver, and (c) the received waveform of the musical composition from the FM-modulation scheme for the atom-based stereo receiver. The top curves are the instrumental part (designated as the left channel), and the bottom curves are the vocal part (designated as the right channel).

waveform, and the output was connected in two different configurations. The first configuration consisted of simply connecting the output of the photodetectors to a set of computer speakers: the output for the ^{133}Cs probe-laser photodetector was connected to left speaker, and the output for the ^{85}Rb probe-laser photodetector was connected to right speaker. In the second configuration, the outputs of the two photodetectors were connected to a stereo jack and plugged into the microphone input of a computer. We then used Audacity to record the left and right channels separately from this microphone input.

More details about how the demodulation is performed are needed. Consider a CW RF signal with no modulation. This RF field will create a change in the EIT signal that is static in time. It will either split the EIT into two peaks (as in Figure 2) for a high field strength or reduce the amplitude of the EIT for lower field strengths [as in Figure 3(a)]. If the probe-laser frequency is fixed to the location of a peak, the transmitted laser power seen on the photodetector will result in a dc value. The EIT/AT effect takes a CW RF field and converts it to a static dc voltage on the photodetector.

Now, if the RF field is modulated in time (through either AM or FM), the EIT or AT peaks will change in time, which will be seen in the transmitted probe-laser power on the photodetector. In the case of AM, either the EIT peak will increase and decrease in amplitude or the AT peaks will move in the probe-laser spectrum. In either case, with the probe-laser frequency fixed, the voltage on the photodetector will oscillate at the modulation rate. In the case of FM, the AT peaks will again shift in the probe-laser spectrum, causing the probe-laser transmission at a fixed optical frequency to oscillate at the modulation rate. In essence, the high-frequency CW RF field that is resonant with the Rydberg transition causes a static shift in the EIT/AT signal, while a modulation of that RF field can be seen in the time domain of the probe-laser transmission on the photodetector. In effect, the atoms demodulate the AM/FM CW carrier, and the baseband signal is simply the output voltage of the photodetector.

EXPERIMENTAL RESULTS

We initially modulated the two different carriers with the same waveform. This ensured that the same baseband signal could be received simultaneously by the two different atomic species (i.e., receiving on both ^{85}Rb and ^{133}Cs at the same time). To accomplish this, we played music through the computer and connected that signal (through the computer stereo headphone jack) to the AM input of two SGs. (The music was in mono, with the same voltage waveform on the left and right channels.) We first observed the output by listening to the left and right speakers. Although there was some noise in the sound the left and right speaker outputs were essentially the same. We then recorded the music (via the microphone input and with Audacity). The outputs of the two channels are not shown here, but they were virtually the same. We used this approach to stream and listen to music for several hours at a time, illustrating the long-term stability of the approach.

To demonstrate stereo reception, we played the instrumental part of the musical composition, shown in the top curve of Figure 5(a), through the left channel (which modulated the 19.626-GHz carrier), and we played the vocal part, shown in bottom curve of Figure 5(a), through the right channel (which modulated the 20.644-GHz carrier). In turn, the baseband of the 19.626-GHz carrier (i.e., the left channel, which contains the instrumental part) was received by the ^{133}Cs atoms, and the baseband of the 20.644-GHz carrier (i.e., the right channel, which contains the vocal part) was received by the ^{85}Rb atoms.

The outputs of the photodetectors for the left and right channels were then connected to the right and left computer speakers, and stereo reception was achieved (and we listened to the musical composition). The output sound from the speakers was of high fidelity, in that the musical composition was clearly audible and very understandable, although some noise was audible (see the "Effects of White Gaussian Noise" section for a discussion of audio-quality assessment). Although noise was present, it had a very minor effect on the quality of the sounds.

We then connected the output of the photodetectors to the microphone jack of the computer and recorded the two channels. These two recordings are shown in Figure 5(b). Compared to the original data file shown in Figure 5(a), these are basically the same files [except for the fact that the data in Figure 5(b) have less amplitude than those in Figure 5(a)]. In Figure 5(b), we do see some clipping (or possible amplitude compression) in the left channel (i.e., the instrumental part), but, although it is visible in the figure, it was not apparent when we listened to the musical composition. To further illustrate the point, Figure 6 shows a 0.59-s segment of the waveforms shown in Figure 5, in

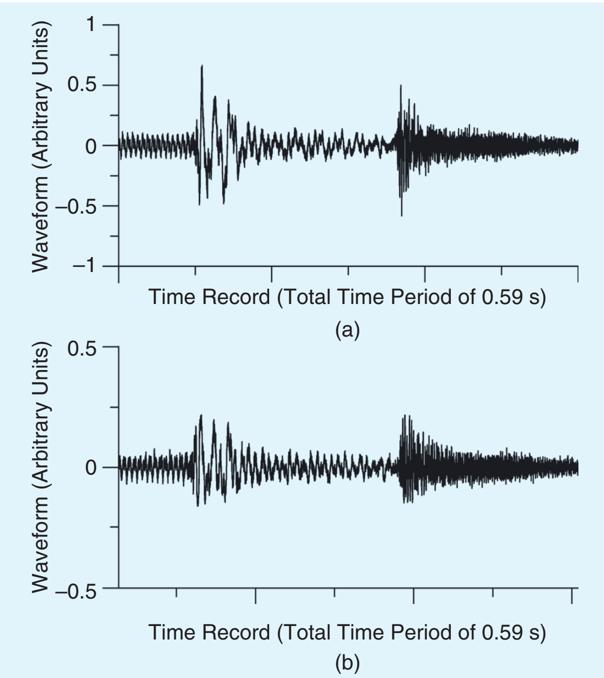

FIGURE 6. A comparison of a 0.59-s segment of the instrumental part of the musical composition showing (a) the transmitted part and (b) the AM received part.

which we compare the transmitted waveform to that received with the AM scheme. Even with the clipping, the waveforms are similar except for the difference in amplitudes; the clipping is due, in part, to the response of the photodetector used for the left channel.

Assessing the quality of audio files is not a trivial task. For digital data, one can analyze either the bit-error rate or the error-vector magnitude (as was done in [29] for phase-modulated signals), but such methods cannot be used for audio data. (See the "Effects of White Gaussian Noise" section for one method of determining audio equality.) With that said, these results illustrated the multiband (or multichannel) receiving capability of a small single-vapor cell.

We next demonstrate the FM scheme by using the computer headphone outputs as the inputs to the FM feature of two SGs. When listening to the output of the two speakers, we noticed that, although there was some more noise than was observed in the AM scheme, high-fidelity music was present. Figure 5(c) shows the received waveform from the atoms using the FM scheme.

The majority of the noise in the data sets for both AM and FM results from laser noise. Although the detection could be improved and laser noise reduced, the results here illustrate the capability of an atom-based multichannel receiver.

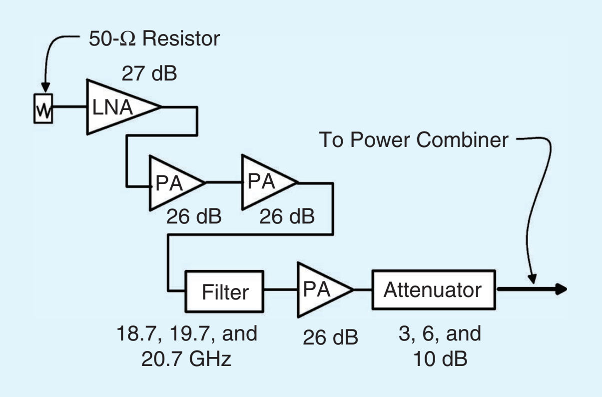

FIGURE 7. A block diagram of the noise source setup. LNA: low-noise amplifier.

TABLE 1. THE CALCULATED CSNR VALUES (RATIO OF THE CW POWER IN THE CARRIER TO INTEGRATED NOISE POWER, BOTH MEASURED AT THE INPUT TO THE HORN ANTENNA) AND NOISE LEVELS IN THE RECEIVED AUDIO SIGNAL (MEAN NOISE LEVEL RELATIVE TO PEAK SIGNAL LEVEL).

Noise Levels	CSNR (linear/dB)	Audio-Noise Level (dB)
Transmitted signal	—	–68.8
Received: no noise	—	–27
Noise conditions (dB attenuator)		
Filter 1: 10	0.056/–12.5	–22.3
Filter 1: 6	0.024/–16.2	–19.5
Filter 1: 3	0.014/–18.5	–14.9
Filter 1: 0	0.0058/–22.4	–8
Filter 2: 10	0.056/–12.5	–23.7
Filter 2: 6	0.025/–16.1	–23.4
Filter 2: 3	0.011/–19.5	–19.9
Filter 2: 0	0.0055/–22.6	–16.8
Filter 3: 10	0.081/–10.9	–23.9
Filter 3: 6	0.032/–14.9	–24
Filter 3: 3	0.017/–17.6	–23.3
Filter 3: 0	0.0081/–20.9	–22.6

The labels for the attenuators (i.e., 3, 6, and 10 dB) are only approximate, and we used measured values to calculate the CSNR values shown in the table.

EFFECTS OF WHITE GAUSSIAN NOISE

For this to be a useful technique, it is important to understand the influence of noise, particularly white Gaussian noise (WGN). In fact, this atom-based approach may be less susceptible to noise. This is confirmed in [20], where we performed experiments measuring CW E-field strengths using this atom-based approach in the presence of band-limited WGN (BLWGN), and we showed that the E-field strength could be detected in low CW-signal-to-noise-power ratio (CSNR) conditions. In this section, we report on some preliminary experiments to investigate how noise affects the reception of AM signals.

For this investigation, we used the right channel of the musical composition (i.e., the vocal part) from the AM scheme. This part is particularly useful because it has gaps of near silence, and these gaps provide good locations to measure any noise that has been added.

In these tests, we injected BLWGN and a modulated carrier into a horn antenna via a power combiner. We used a similar noise source as that used in [20]; details on how the noise was generated are provided in [20], and a diagram is shown in Figure 7. The noise source includes a 50-Ω resistor series with a low-noise amplifier (having a gain of 27 dB) and two power amplifiers (PAs), each having a gain of 26 dB. The output of the second PA was sent to three different bandpass filters (changed during the experiment to generate different noise spectra). The three different center frequencies are as follows (each filter had a bandwidth of 1 GHz): filter 1 was ≈20.7 GHz, filter 2 was ≈19.7 GHz, and filter 3 was ≈18.7 GHz. The noise-power spectral densities for these bandpass filters are shown in [20, Fig. 5]. The measured integrated noise power (total power over the filter bandwidth measured with a power meter) for each filter used was 0.40 dBm for filter 1, 0.55 dBm for filter 2, and –1.10 dBm for filter 3.

To vary the noise levels during the experiments, we added one of three different attenuators between the noise source and the power combiner. This provided a total of four different BLWGN levels for each of the three filters (one without an attenuator and one for each of three different attenuators). The CSNRs (defined as the ratio of the CW power in the carrier to the integrated noise power, both measured at the input to the horn antenna) for these different combinations are shown in Table 1. During the experiment, the 20.64-GHz carrier at the output of the power combiner was –22.0 dBm.

Across the 13 different cases (no noise added and four added noise levels, each crossed with three filters), the vocal signal was never noticeably distorted. However, the noise present in the received audio signal ranged from minor to severe. We measured the noise levels in the silent intervals of the received audio signal and report the results here.

Measuring noise levels involves comparing the recorded audio files with the original transmitted audio file. The first step is to use correlation to find and remove the time shift between the transmitted audio file and each received audio file. We then segmented each file into groups of N = 1,024 audio samples (called *frames*) and calculated the power in decibels for each frame. We used an audio sample rate of 48,000 sample/s, so each frame has a duration of 21.3 ms. The power of the ith frame is given by

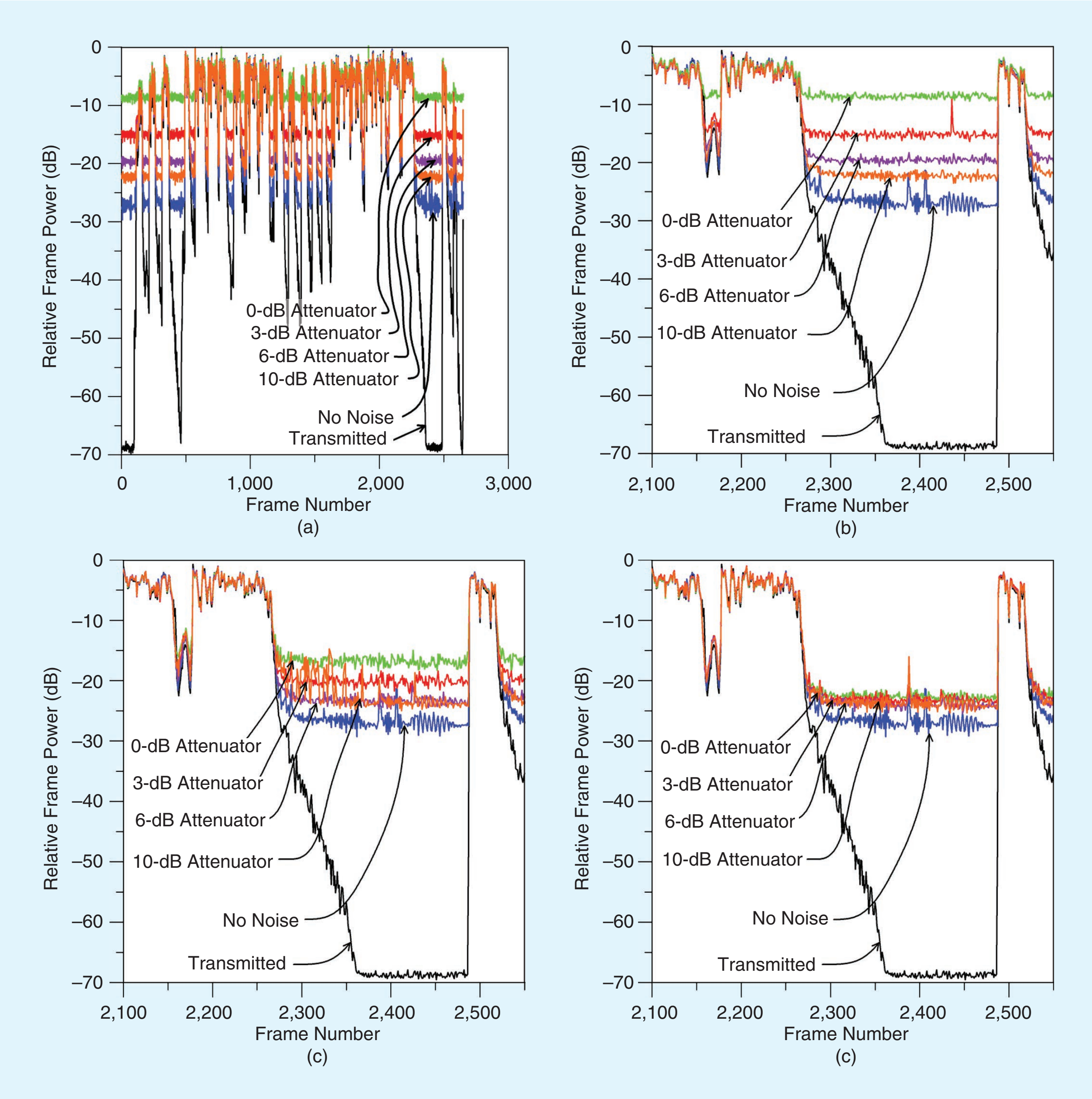

FIGURE 8. The frame power histories: (a) the full record for filter 1 and partial records for filters (b) 1, (c) 2, and (d) 3.

$$P_i = 10\log_{10} \sum_{j=1}^{N} x^2_{(i-1)N+j}, \quad (2)$$

where x_k represents the kth data point in the entire audio sample.

We produced frame power histories for each of the 13 cases and for the original transmitted audio file as well. We normalized each history to have a power of 0 dB at frame 573, the frame of the transmitted audio file that has the greatest power. (Each of the other 13 signals has maximal frame power at frame 573 as well.) This normalization step is equivalent to matching the levels of each of the received audio signals with the level of the transmitted audio signal. This is required to make meaningful comparisons between the noise levels associated with each of the signals.

These frame power histories are shown Figure 8. Figure 8(a) shows the entire history (approximately 77 s) for filter 1. The effect of the noise is easily seen by viewing a portion of the history, as in Figure 8(b)–(d). Each of these shows approximately 450 frames (10 s) for one of the three filters, illustrating how a gap in the vocal signal provides an opportunity to measure noise levels. Thanks to normalization, the histories are very similar when the vocal signal is present (e.g., frames 2,200–2,250). However, when the vocal signal is absent (e.g., frames 2,400–2,450), the noise induced into the received audio by the added RF noise is clearly evident.

Figure 8 shows that, as expected, lower levels of added RF noise power produce lower levels of noise in the received audio. The figure also shows that the effect of added RF noise is strongest in the case of filter 1 and weakest in the case of filter 3. That is, the noise that is blue-shifted from the carrier (filter 1) has the most effect. This is consistent with noise experiments in other studies, where it was shown that blue-shifted noise has the strongest effect on E-field strength measurements performed with the EIT/AT approach [20].

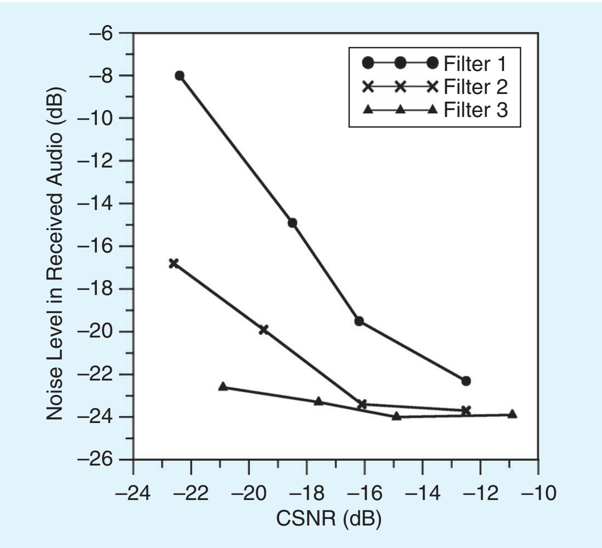

FIGURE 9. The audio-noise levels (relative to the peak signal level) versus CSNR values.

Although Figure 8 provides intuitive and accessible illustrations of these effects, more quantitative results are provided in Table 1 and Figure 9. To obtain these results, we averaged frame powers over 200 frames (approximately 4 s) where no vocal signal was present. These average audio-noise frame power values are relative to the peak level of the vocal signal combined with the noise. Using the fact that the vocal signal power and noise power are additive, we then adjusted each average audio-noise frame power value to report the audio-noise level in decibels relative to the peak signal level. These audio-noise levels, along with the corresponding CSNR values, are given in Table 1 and Figure 9.

When no interfering RF noise is presented at the vapor cell, the audio-noise level is 27 dB down. This noise is audible in a quiet listening environment but would be inaudible in a typical office, retail, or automotive environment. As more interfering RF noise is introduced, the measured audio-noise level increases, and the perceived severity of that noise increases accordingly. For this specific signal and noise combination, noise levels of approximately –20 dB may be perceived and described as "moderate," whereas levels near –10 dB would likely be described as "severe." Figure 9 shows quantitatively how, given a fixed CSNR, noise from filter 1 is much more detrimental than noise from filter 2, which, in turn, is slightly more detrimental than that from filter 3. In addition, Figure 9 suggests the presence of an inflection point, perhaps approximately –15 dB CSNR. It appears that below this point, changes in CSNR have greater influence in received audio-noise level, while, above this point, changes in CSNR exert a lesser influence.

FUTURE WORK ON MODULATION DETECTION

We continued these noise studies by transmitting and receiving a 511-b pseudorandom bit stream using both AM and FM signals where we show bit-error rates for various data rates and BLWGN levels. The results demonstrate that, although noise is observed in the data, the signal quantity of the received signal is, for the most part, immune to the noise, even for low values of CSNR (high noise levels). This study also shows that the Rydberg atom receiver has a bandwidth of approximately 1–5 MHz (which is independent of the carrier frequency of hundreds of MHz–1 THz). This bandwidth limit is also confirmed in [26] and [29] and is due to the time required to populate the atoms to a Rydberg state [29].

Although the results in this article demonstrated the ability to detect AM and FM signals, the modulation scheme for digital communications most widely used today is phase-shift keying (PSK) and quadrature PSK (QPSK) [29]. In these modulation schemes, data are transmitted by changing (or modulating) the phase of the CW carrier. QPSK is a type of PSK (where two bits are modulated at the same time) performed by choosing one of four possible phases applied to a CW carrier (e.g., 45°, 135°, 225°, and 315°). Thus, to receive QPSK signals, one needs to measure and detect the phases of the CW carrier.

Recently, in [28], we introduced a Rydberg atom-based mixer and described a method for measuring the phase of an RF field using Rydberg atoms as a mixer to downconvert an RF field at 20 GHz to an intermediate frequency on the order of kilohertz. (The phase of the intermediate frequency corresponds directly to the phase of the RF field.) In [28] and [38], we demonstrated the ability to measure the propagation constant of a plane wave in free space to within 1% when compared to theoretical values. The Rydberg atom-based mixer also allows us to measure weak E-filed values (<40 μV/m) with subhertz frequency resolution as well as detect and receive digitally modulated signals (e.g., binary PSK, QPSK, and quadrature AM). Both of these topics are covered in separate publications [28], [29], [37], and [38]. Field enhancement techniques can also be used for weak-field detection [39]. Finally, we used this atom receiver to perform a real-time recording of a musical instrument [24].

DISCUSSION AND CONCLUSIONS

Rydberg atom-based receivers/sensors are a new area of research, and this type of scheme potentially has many advantages over conventional receiving and detection technologies. In this article, we discussed the ability of atom-based technologies to receive multiple channels simultaneously. We presented one realization of this using two different atomic species (^{85}Rb and ^{133}Cs) simultaneously to receive a stereo musical composition using both AM and FM schemes. The output heard from the speakers had a small amount of noise but was of high fidelity, in that the musical composition was clearly audible and very understandable.

We also investigated the effects of BLWGN on the ability to receive these AM/FM signals. Generally, the received signals are not noticeably distorted by the various noise levels (i.e., even for CSNR as low as –22 dB). In fact, the BLWGN does not cause distortion, but it can cause very audible noise in the received audio signal, depending on the CSNR. In effect, the atoms act as a filter for the noise.

This type of atom-based receiver/sensor potentially has several advantages. The most noticeable are as follows:

- The atoms perform the demodulation and allow for direct readout of the baseband signal
- They allow for multiband (multichannel) receiving in one sensor head.
- One sensor head can operate from hundreds of megahertz to 1 THz.
- The bandwidth of operation is limited to approximately 5 MHz, but this bandwidth is constant over the entire frequency range of hundreds of megahertz to 1 THz.

One might ask, "How does a Rydberg atom-based system compare to a conventional receiving system?" To answer this question, we must remember that the Rydberg atom-based receiver replaces the receiving antenna and front-end components and electronics used in a conventional receiver system. For example, the Rydberg atoms perform some of the same functions as both antennas and demodulators, and this must be considered when comparing the receiver with traditional systems. This is not an easy thing to answer. Our group and other investigators are in the process of researching the best methods for comparing a Rydberg atom-based receiver system to conventional systems and identifying the best performance metrics for this new type of receiver.

We can make a few initial statements to address these points. A traditional receiver consists of an antenna, amplifier, and demodulator to retrieve the baseband signal. Hence, antenna and electronics performance are decoupled and can be specified separately. The Rydberg atom receiver replaces two or more of these functions with an atomic-vapor cell and its optical readout of the atomic response to the RF radio wave. In its simplest form, no receiver antenna is needed; in this case, the atomic receiver directly reads the RF E-field and its modulation.

The Rydberg atom-based field-sensing approach has the advantage of working over a large dynamic range, where field values down to 40 μV/m and as high as 10 kV/m have been demonstrated [4], [37]–[39]. For weak fields, one may need to use metallic structures for field enhancement [39] and/or use a mixer-type approach [37]. For high field strengths, one may need to use the ac Stark shift method [12] or a Floquet method [11]. Both the weak-field and high-field approaches have been shown to be very successful in detecting both fields and modulated signals. For weak-field detection, it is also instructive to discuss the detectable power density. The estimated sensitivity of 40 μV/m corresponds to –87 dBm/m^2, which, for an isotropic transmitter with 1 W of power, corresponds to a range near 200 km.

Nonlinearities in the received signals are possible and can be quantitatively traced back to the various modes of atomic response (linear ac Stark shifts, quadratic ac Stark shifts, and high-field Floquet spectra). The atomic nonlinearities cause higher harmonics in the received signal. A quantitative study of harmonic distortion and potential remedies may be addressed in future work. Inspection of Figure 9 further indicates that the present system has a dynamic range on the order of 25 dB, without added RF noise. This is close to the typical AM radio dynamic range.

The Rydberg atom-based sensor behaves fundamentally differently than does a conventional antenna, and, as such, it is not straightforward to characterize the Rydberg atom sensor in the same way one characterizes a conventional antenna. The sensing of the E-field is performed with an optical transmission through a vapor cell, which detects the magnitude of the field. However, metallic structures can be used to enhance the sensitivity or polarization selectively. This is done by either placing metal structures inside the vapor cell [39] or embedding the vapor cell inside waveguiding structures [38]. In fact, there are a few ways to detect polarization of the RF field. One method is based on the atomic states used and the relative difference between the polarization of the optical fields and the incident RF field [6]. Polarization selectivity can also be achieved by incorporating metallic structures with the vapor cell [38], [39].

The atom-based sensor interacts with noise in a fundamentally different way than conventional systems, which means that a Rydberg atom-based sensor/receiver may be more immune to noise. The results presented here and those given in [20] indicated that E-field strengths and modulated signals could be measured and detected in the presence of BLWGN for low CSNR conditions. Although this point is currently being investigated in detail, we can make the following comments.

In the atomic receiver, there is technical noise on the elements, which include the vapor cell, lasers, and photodiode. The technical noise includes laser fluctuations, vibrations in the setup, and electronic noise in the photodiode as well as added noise in the transimpedance amplifier that converts the photocurrent into a voltage. In addition, there is fundamental noise, such as photon shot noise, in the photodiode signals. Usually, the noise-equivalent power of the photodiode/transimpedance amplifier unit greatly exceeds the photon shot noise of the probe laser. There is also RF noise from the environment, such as unwanted radio signals and so on, that may perturb the atoms' responses to the modulated carrier. In the present case, we studied only the last aspect in detail (see the "Effects of White Gaussian Noise" section).

When new technology first emerges, the cost the of the system can be high. As the technology evolves and becomes used and accepted, however, the cost of the system decreases. In fact, several private companies are currently investigating and developing the needed components for this technology. As the appropriate metrics for evaluating the performance of these atom-based receivers are developed, comparisons with the size, weight, power, and cost (SWAPC) requirements can be investigated. Because of the numerous potential applications of this new sensor technology, several groups around the world have begun programs in the area of Rydberg atom-based sensors/receivers, including universities, private companies, government agencies, and most national metrology institutes around the world.

AUTHOR INFORMATION

Christopher L. Holloway (christopher.holloway@nist.gov) is with the National Institute of Standards and Technology, Boulder, Colorado. He is a Fellow of the IEEE.

Matthew T. Simons (matthew.simons@nist.gov) is with the National Institute of Standards and Technology, Boulder, Colorado. He is a Member of the IEEE.

Abdulaziz H. Haddab (haddab@colorado.edu) is with the National Institute of Standards and Technology, Boulder, Colorado. He is a Student Member of the IEEE.

Joshua A. Gordon (josh.gordon@nist.gov) is with the National Institute of Standards and Technology, Boulder, Colorado. He is a Senior Member of the IEEE.

David A. Anderson (dave@rydbergtechnologies.com) is with Rydberg Technologies, LLC, Ann Arbor, Michigan. He is a Member of the IEEE.

Georg Raithel (graithel@umich.edu) is with Rydberg Technologies, LLC, and the Department of Physics, University of Michigan, both in Ann Arbor.

Stephen D. Voran (svoran@ntia.doc.gov) is with the Institute for Telecommunication Sciences, Boulder, Colorado. He is a Senior Member of the IEEE.

REFERENCES

[1] T. F. Gallagher, *Rydberg Atoms*. Cambridge, U.K.: Cambridge Univ. Press, 1994.
[2] C. L. Holloway et al., "Atom-based RF electric field metrology: From self-calibrated measurements to sub-wavelength and near-field imaging," *IEEE Trans. Electromagn. Compat.*, vol. 59, no. 2, pp. 717–728, 2017. doi: 10.1109/TEMC.2016.2644616.
[3] C. L. Holloway et al., "Broadband Rydberg atom-based electric-field probe for SI-traceable, self-calibrated measurements," *IEEE Trans. Antenna Propag.*, vol. 62, no. 12, pp. 6169–6182, 2014. doi: 10.1109/TAP.2014.2360208.
[4] J. A. Sedlacek, A. Schwettmann, H. Kubler, R. Low, T. Pfau, and J. P. Shaffer, "Microwave electrometry with Rydberg atoms in a vapour cell using bright atomic resonances," *Nat. Phys.*, vol. 8, no. 11, pp. 819–824, 2012. doi: 10.1038/nphys2423.
[5] C. L. Holloway et al., "Sub-wavelength imaging and field mapping via electromagnetically induced transparency and Autler-Townes splitting in Rydberg atoms," *Appl. Phys. Lett.*, vol. 104, no. 24, pp. 244102-1–244102-5, 2014. doi: 10.1063/1.4883635.
[6] J. A. Sedlacek, A. Schwettmann, H. Kubler, and J. P. Shaffer, "Atom-based vector microwave electrometry using rubidium Rydberg atoms in a vapor cell," *Phys. Rev. Lett.*, vol. 111, no. 6, p. 063001, 2013. doi: 10.1103/PhysRevLett.111.063001.
[7] J. A. Gordon et al., "Millimeter wave detection via Autler-Townes splitting in rubidium Rydberg atoms," *Appl. Phys. Lett.*, vol. 105, no. 2, p. 024104, 2014. doi: 10.1063/1.4890094.
[8] H. Fan, S. Kumar, J. Sedlacek, H. Kubler, S. Karimkashi, and J. P. Shaffer, "Atom based RF electric field sensing," *J. Phys. B, At. Mol. Opt. Phys.*, vol. 48, no. 20, p. 202,001, 2015. doi: 10.1088/0953-4075/48/20/202001.
[9] M. Tanasittikosol et al., "Microwave dressing of Rydberg dark states," *J. Phys B, At. Mol. Opt. Phys.*, vol. 44, no. 18, p. 184,020, 2011. doi: 10.1088/0953-4075/44/18/184020.
[10] C. G. Wade, N. Sibalic, N. R. de Melo, J. M. Kondo, C. S. Adams, and K. J. Weatherill, "Real-time near-field terahertz imaging with atomic optical fluorescence," *Nat. Photonics*, vol. 11, no. 1, pp. 40–43, 2017. doi: 10.1038/nphoton.2016.214.
[11] D. A. Anderson, S. A. Miller, G. Raithel, J. A. Gordon, M. L. Butler, and C. L. Holloway, "Optical measurements of strong microwave fields with Rydberg atoms in a vapor cell," *Phys. Rev. Appl.*, vol. 5, no. 3, p. 034003, 2016. doi: 10.1103/PhysRevApplied.5.034003.
[12] D. A. Anderson, E. Paradis, G. Raithel, R. E. Sapiro, and C. L. Holloway, "High-resolution antenna near-field imaging and sub-THz measurements with a small atomic vapor-cell sensing element," in *Proc. 2018 11th Global Symp. Millimeter Waves (GSMM)*, Boulder, CO, pp. 1–3. doi: 10.1109/GSMM.2018.8439437.
[13] D. A. Anderson et al., "Two-photon microwave transitions and strong-field effects in a room-temperature Rydberg atom gas," *Phys. Rev. A*, vol. 90, no. 4, p. 043419, 2014. doi: 10.1103/PhysRevA.90.043419.
[14] A. K. Mohapatra, T. R. Jackson, and C. S. Adams, "Coherent optical detection of highly excited Rydberg states using electromagnetically induced transparency," *Phys. Rev. Lett.*, vol. 98, no. 11, p. 113,003, 2007. doi: 10.1103/PhysRevLett.98.113003.
[15] C. L. Holloway, M. T. Simons, J. A. Gordon, A. Dienstfrey, D. A. Anderson, and G. Raithel, "Electric field metrology for SI traceability: Systematic measurement uncertainties in electromagnetically induced transparency in atomic vapor," *J. Appl. Phys.*, vol. 121, no. 23, p. 233,106, 2017. doi: 10.1063/1.4984201.
[16] M. T. Simons, J. A. Gordon, C. L. Holloway, D. A. Anderson, S. A. Miller, and G. Raithel, "Using frequency detuning to improve the sensitivity of electric field measurements via electromagnetically induced transparency and Autler-Townes splitting in Rydberg atoms," *Appl. Phys. Lett.*, vol. 108, no. 17, p. 174,101, 2016. doi: 10.1063/1.4947231.
[17] M. T. Simons, J. A. Gordon, and C. L. Holloway, "Simultaneous use of Cs and Rb Rydberg atoms for dipole moment assessment and RF electric field measurements via electromagnetically induced transparency," *J. Appl. Phys.*, vol. 120, no. 12, p. 123,103, 2016. doi: 10.1063/1.4963106.
[18] C. L. Holloway, M. T. Simons, M. D. Kautz, A. H. Haddab, J. A. Gordon, and T. P. Crowley, "A quantum-based power standard: Using Rydberg atoms for a SI-traceable radio-frequency power measurement technique in rectangular waveguides," *Appl. Phys. Lett.*, vol. 113, no. 9, p. 094101, 2018. doi: 10.1063/1.5045212.

[19] M. T. Simons, J. A. Gordon, and C. L. Holloway, "Fiber-coupled vapor cell for a portable Rydberg atom-based radio frequency electric field sensor," *Appl. Opt.*, vol. 57, no. 22, pp. 6456–6460, 2018. doi: 10.1364/AO.57.006456.
[20] M. T. Simons, M. D. Kautz, C. L. Holloway, D. A. Anderson, and G. Raithel, "Electromagnetically induced transparency (EIT) and Autler-Townes (AT) splitting in the presence of band-limited white Gaussian noise," *J. Appl. Phys.*, vol. 123, no. 20, p. 203,105, 2018. doi: 10.1063/1.5020173.
[21] D. H. Meyer, K. C. Cox, F. K. Fatemi, and P. D. Kunz, "Digital communication with Rydberg atoms and amplitude-modulated microwave fields," *Appl. Phys. Lett.*, vol. 112, no. 21, p. 211,108, 2018. doi: 10.1063/1.5028357.
[22] K. C. Cox, D. H. Meyer, F. K. Fatemi, and P. D. Kunz, "Quantum-limited atomic receiver in the electrically small regime," *Phys. Rev. Lett.*, vol. 121, no. 11, p. 110,502, 2018. doi: 10.1103/PhysRevLett.121.110502.
[23] D. A. Anderson, R. E. Sapiro, and G. Raithel, An atomic receiver for AM and FM radio communication. Aug. 26, 2018. [Online]. Available: arXiv:1808.08589v1
[24] C. L. Holloway, M. T. Simons, A. H. Haddab, C. J. Williams, and M. W. Holloway, "A 'real-time' guitar recording using Rydberg atoms and electromagnetically induced transparency: Quantum physics meets music," *AIP Adv.*, vol. 9, no. 6, p. 065110, 2019. doi: 10.1063/1.5099036.
[25] A. B. Deb and N. Kjaergaard, "Radio-over-fiber using an optical antenna based on Rydberg states of atoms," *Appl. Phys. Lett.*, vol. 112, no. 21, p. 211,106, 2018. doi: 10.1063/1.5031033.
[26] Z. Song et al., "Rydberg-atom-based digital communication using a continuously tunable radio-frequency carrier," *Opt. Express*, vol. 27, no. 6, pp. 8848–8857, 2019. doi: 10.1364/OE.27.008848.
[27] "Get ready for atom radio," *MIT Technology Review,* June 2018. [Online]. Available: https://www.technologyreview.com/s/611977/get-ready-for-atomic-radio/
[28] M. T. Simons, A. H. Haddab, J. A. Gordon, and C. L. Holloway, "A Rydberg atom-based mixer: Measuring the phase of a radio frequency wave," *Appl. Phys. Lett.*, vol. 114, no. 11, p. 114,101, 2019. doi: 10.1063/1.5088821.
[29] C. L. Holloway, M. T. Simons, A. H. Haddab, and J. A. Gordon, "Detecting and receiving phase-modulated signals with a Rydberg atom-based receiver," *IEEE Antennas Wireless Propag. Lett.*, vol. 18, no. 9, pp. 1853–1857, 2019. doi: 10.1109/LAWP.2019.2931450.
[30] J. Kitching, "Chip-scale atomic devices," *Appl. Phys. Rev.*, vol. 5, no. 3, p. 031302, 2018. doi: 10.1063/1.5026238.
[31] Z. L. Newman et al., "Architecture for the photonic integration of an optical atomic clock," *Optica*, vol. 6, no. 5, pp. 680–685, 2019. doi: 10.1364/OPTICA.6.000680.
[32] M. Stock, "The revision of the SI-towards an International System of Units based on defining constants," *Meas. Techn.*, vol. 60, no. 12, pp. 1169–1177, 2018. doi: 10.1007/s11018-018-1336-2.
[33] "Road to the revised SI," National Institute of Standards and Technology (NIST), Gaithersburg, MD, 2019. [Online]. Available: https://www.nist.gov/si-redefinition/road-revised-si
[34] Queen, "Under Pressure," featuring D. Bowie, by F. Mercury, B. May, R. Taylor, J. Deacon, and D. Bowie, track 11 on *Hot Space*, EMI-Elektra, May 21, 1982.
[35] C. L. Holloway, M. T. Simons, M. Kautz, P. F. Wilosn, and J. A. Gordon, "Development and applications of a fiber-coupled atom-based electric field probe," in *Proc. Int. Symp. Electromagnetic Compatibility (EMC Europe 2018)*, Amsterdam, The Netherlands, Aug. 27–30, 2018, pp. 381–385. doi: 10.1109/EMCEurope.2018.8485006.
[36] D. A. Steck, "Rubidium 85 D line data revision 2.1.6," Sept. 20, 2013. [Online]. Available: http://steck.us/alkalidata
[37] J. A. Gordon, M. T. Simons, and C. L. Holloway, "Weak electric-field detection with sub-1 Hz resolution at radio frequencies using a Rydberg atom-based mixer," *AIP Adv.*, vol. 9, no. 4, p. 045030, 2019. doi: 10.1063/1.5095633.
[38] M. T. Simons, A. H. Haddab, J. A. Gordon, D. Novotny, and C. L. Holloway, "Embedding a Rydberg atom-based sensor into an antenna for phase and amplitude detection of radio-frequency fields and modulated signals," *IEEE Access*, vol. 7, pp. 164,975–164,985, Oct. 2019. doi: 10.1109/ACCESS.2019.2949017.
[39] D. A. Anderson, E. G. Paradis, and G. Raithel, "A vapor-cell atomic sensor for radio-frequency field detection using a polarization-selective field enhancement resonator," *Appl. Phys. Lett.*, vol. 113, p. 073501, Aug. 2018. doi: 10.1063/1.5038550.